

Article

Genome-Wide Identification of the Ferric Chelate Reductase (*FRO*) Gene Family in Peanut and Its Diploid Progenitors: Structure, Evolution, and Expression Profiles

Junhua Guan, Zheng Zhang and Gangrong Shi *

College of Life Sciences, Huaibei Normal University, Huaibei 235000, China; 12111070719@chnu.edu.cn (J.G.); swx@chnu.edu.cn (Z.Z.)

Abstract: The ferric chelate reductase (*FRO*) family plays a vital role in metal ion homeostasis in a variety of locations in the plants. However, little is known about this family in peanut (*Arachis hypogaea*). This study aimed to identify *FRO* genes from the genomes of peanut and the two diploid progenitors (*A. duranensis* and *A. ipaensis*) and to analyze their gene/protein structures and evolution. In addition, transcriptional responses of *AhFRO* genes to Fe deficiency and/or Cu exposure were investigated in two peanut cultivars with different Fe deficiency tolerance (Silihong and Fenghua 1). A total of nine, four, and three *FRO* genes were identified in peanut, *A. duranensis*, and *A. ipaensis*, respectively, which were divided into three groups. Most *AhFRO* genes underwent WGD/segmental duplication, leading to the expansion of the *AhFRO* gene family. In general, clustered members share similar gene/protein structures. However, significant divergences occurred in *AhFRO2* genes. Three out of five *AhFRO2* genes were lowly expressed in all tissues under normal conditions, which may be beneficial for avoiding gene loss. Transcription analysis revealed that *AhFRO2* and *AhFRO7* genes might be involved in the reduction of Fe/Cu in plasma membranes and plastids, respectively. *AhFRO8* genes appear to confer Fe reduction in the mitochondria. Moreover, Fe deficiency induced an increase of Cu accumulation in peanut plants in which *AhFRO2.2/2.4/2.5* and *FRO7.1/7.2* might be involved. Our findings provided new clues for further understanding the roles of *AhFRO* genes in the Fe/Cu interaction in peanut.

Keywords: *Arachis hypogaea*; *FRO*; cultivar; Fe deficiency; Cu accumulation



Citation: Guan, J.; Zhang, Z.; Shi, G. Genome-Wide Identification of the Ferric Chelate Reductase (*FRO*) Gene Family in Peanut and Its Diploid Progenitors: Structure, Evolution, and Expression Profiles. *Plants* **2024**, *13*, 418. <https://doi.org/10.3390/plants13030418>

Academic Editor: Stanislav Isayenkov

Received: 5 December 2023

Revised: 17 January 2024

Accepted: 29 January 2024

Published: 31 January 2024



Copyright: © 2024 by the author. Licensee MDPI, Basel, Switzerland. This article is an open access article distributed under the terms and conditions of the Creative Commons Attribution (CC BY) license (<https://creativecommons.org/licenses/by/4.0/>).

1. Introduction

Iron (Fe) is a microelement that is essential for plant growth and development. In plants, Fe functions as a constituent of many important molecules such as Fe-sulfur (Fe-S) and heme Fe proteins, which are involved in fundamentally biological processes, including respiration, photosynthesis, chlorophyll biosynthesis, sulfur assimilation, and nitrogen fixation [1]. The function of Fe is mainly based on the reversible redox reaction of ferrous (Fe²⁺) and ferric (Fe³⁺) ions and its ability to form octahedral complexes with various ligands. Fe deficiency not only inhibits chlorophyll synthesis and reduces photosynthetic efficiency [2] but also interrupts the respiratory electron transport and tricarboxylic acid cycle [3]. Meanwhile, Fe in excess can be toxic because free Fe ions induce the formation of reactive oxygen species via the Fenton reaction [4,5]. Therefore, cellular Fe levels must be strictly controlled in plants.

Although Fe is the fourth most abundant element in the earth's crust, it is not easily taken up by plants due to the predominance of insoluble ferric oxides in soils, particularly in calcareous soils that account for approximately 30% of the world's arable soils [6]. Consequently, crops grown in calcareous soils often suffer from iron deficiency, limiting yield and quality. Moreover, Fe deficiency in plants also poses serious health problems because plant foods are the main source of dietary Fe for humans. It is estimated that 30%–50% of anemia in children and other groups is caused by iron deficiency [7]. Thus,

understanding plant iron homeostasis is essential for improving crop yield and human iron nutrition.

Plants have evolved complex mechanisms to sense and respond to iron fluctuations in the rhizosphere and prevent iron deficiency or toxicity by maintaining Fe homeostasis [4,5,8]. Non-gramineous plants use the reduction strategy (strategy I) for Fe acquisition, while gramineous plants adopt the chelation strategy (strategy II). The reduction strategy includes three processes: (i) releasing protons from root cells to the rhizosphere via H⁺-ATPase for reducing soil pH value; (ii) reducing Fe³⁺ to Fe²⁺ by ferric chelate reductases (FRO) in the acidifying rhizosphere; and (iii) taking up Fe²⁺ into root cells through iron-regulated transporter 1 (IRT1) in the plasma membrane. Gramineous plants can secrete the mugenic acids (MAs) like phytosiderophores from their roots to the soil to dissolve Fe³⁺ in the rhizosphere to form a Fe³⁺-MA complex and then absorb the Fe³⁺-MA complex into root cells through yellow stripe like protein (YSL) in the plasma membrane.

The FRO family plays a vital role in metal ion homeostasis in a variety of locations in plants [9]. It belongs to the flavocytochrome superfamily that transfers electrons across membranes [10]. FRO proteins contain eight transmembrane helices and share three typical domains, a heme-containing ferric reductase domain (PF01794) in the transmembrane region, and the FAD-binding (PF08022) and NAD-binding (PF08030) domains inside the membrane of the C-terminal region [11,12]. In *Arabidopsis*, AtFRO2 is responsible for the reduction of solubilized Fe³⁺ to Fe²⁺ at the root surface, where Fe²⁺ is then transported into the cytoplasm via AtIRT1 in the root plasma membrane [10,13]. AtFRO6 mediates the reduction of Fe³⁺ to Fe²⁺ at the plasma membrane of leaf cells [9,14]. AtFRO7 plays a role in chloroplast iron acquisition by reducing Fe³⁺ to Fe²⁺ [15,16]. AtFRO3 and AtFRO8 have been predicted to localize to mitochondrial membranes and might serve an analogous function in the mitochondrial iron homeostasis [16,17]. While several FRO genes were functionally characterized in *Arabidopsis*, little is known about the roles of this family in other plant species including peanut (*Arachis hypogaea* L.), a major oil-seed crop mainly grown in temperate and tropical regions of the world.

In this study, based on the whole-genome sequences [18,19], FRO family genes of the peanut (cv. Tifrunner) and the two wild ancestral species (*A. duranensis* and *A. ipaënsis*) were identified, and the structures, functions and evolutionary relationships were characterized. Moreover, the expression of *AhFRO* genes in response to Fe deficiency and/or Cu exposure was investigated. Our data would provide a basis for further functional characterization of *AhFROs* and shed new light on the possible roles of the *AhFRO* family in the uptake and translocation of Fe and Cu in plants.

2. Results

2.1. Identification and Phylogenetic Analysis of FRO Genes in the Three *Arachis* Species

Analysis of BLASTp using AtFROs as queries resulted in 26, 14, and 11 non-redundant protein sequences from genomes of *A. hypogaea* cv. Tifrunner, *A. duranensis*, and *A. ipaënsis*, respectively. Phylogenetic analysis indicated that these proteins were divided into two clades: one including all eight AtFRO members could be considered as the FRO family, and the other might be respiratory burst oxidases (Figure S1). A total of nine putative *AhFRO* genes were identified in peanut, including five *AhFRO2* (*AhFRO2.1/2.2/2.3/2.4/2.5*), two *AhFRO7* (*AhFRO7.1/7.2*), and two *AhFRO8* (*AhFRO8.1/8.2*, Table 1). Meanwhile, five *AdFRO* (*AdFRO2.1/2.2/2.3*, *AdFRO7*, and *AdFRO8*) and three *AiFRO* (*AiFRO2*, *AdFRO7*, and *AdFRO8*) genes were identified from *A. duranensis* and *A. ipaënsis*, respectively (Figure S1 and Table 1).

Table 1. Molecular characterization of *FRO* genes and corresponding proteins identified in *A. hypogaea*, *A. duranensis*, and *A. ipaënsis*.

Gene Name	Gene ID	Gene Length (bp)	CDS (bp)	MW ^a (kDa)	aa ^b	Instability	Aliphatic Index	GRAVY ^c	pI ^d	No. of TMD ^e	Location
<i>AhFRO2.1</i>	112732410	2550	2184	81.95	727	39.95	109.13	0.368	9.38	10	PM ^f
<i>AhFRO2.2</i>	112797510	2585	2214	83.53	737	40.69	106.85	0.187	9.47	10	PM
<i>AhFRO2.3</i>	112726301	2417	2187	82.15	728	39.81	109.52	0.348	9.25	10	PM
<i>AhFRO2.4</i>	114925155	1254	702	25.97	233	47.64	99.57	0.011	5.82	2	PM
<i>AhFRO2.5</i>	112744178	2659	2184	82.42	727	40.16	107.11	0.186	9.45	10	PM
<i>AhFRO7.1</i>	112796104	2999	2208	82.84	735	40.35	106.29	0.355	8.31	12	Chlo. ^g
<i>AhFRO7.2</i>	112741396	2842	2217	83.11	738	41.04	105.60	0.324	8.14	12	Chlo.
<i>AhFRO8.1</i>	112702502	2590	1893	70.86	630	46.08	109.13	0.333	9.16	8	Mito. ^h
<i>AhFRO8.2</i>	112765774	2463	2124	79.36	707	45.57	112.43	0.377	9.30	11	Mito.
<i>AdFRO2.1</i>	107472727	2407	2184	82.06	727	39.57	108.46	0.359	9.39	10	PM
<i>AdFRO2.2</i>	107485816	1056	711	26.40	236	48.31	111.48	0.244	8.23	2	PM
<i>AdFRO2.3</i>	110280250	556	372	13.52	123	35.36	91.87	−0.129	6.82	0	PM
<i>AdFRO7</i>	107483074	2508	2217	83.14	738	40.63	105.85	0.347	8.31	12	Chlo.
<i>AdFRO8</i>	107457844	2413	2124	79.45	707	44.89	111.88	0.371	9.28	10	Mito.
<i>AiFRO2</i>	107635065	2710	2184	82.49	727	40.44	107.11	0.181	9.42	10	PM
<i>AiFRO7</i>	107638776	2887	2220	83.21	739	41.14	105.98	0.329	8.14	12	Chlo.
<i>AiFRO8</i>	107609299	2446	2124	79.36	707	45.57	112.43	0.377	9.30	11	Mito.

^a Molecular weight, ^b amino acid number, ^c grand average of hydropathicity, ^d isoelectric points, ^e transmembrane domain, ^f plasma membrane, ^g chloroplast, ^h mitochondria.

The length of *FRO* genes varied from 1254 bp (*AhFRO2.4*) to 2999 bp (*AhFRO7.1*), from 556 bp (*AdFRO2.3*) to 2508 bp (*AdFRO7*), and from 2446 bp (*AiFRO8*) to 2887 bp (*AiFRO7*) for *A. hypogaea*, *A. duranensis*, and *A. ipaënsis*, respectively. The CDS length varied from 702 bp (*AhFRO2.4*) to 2217 bp (*AhFRO7.2*), from 372 bp (*AdFRO2.3*) to 2217 bp (*AdFRO7*), and from 2124 bp (*AiFRO8*) to 2220 bp (*AiFRO7*) for *A. hypogaea*, *A. duranensis*, and *A. ipaënsis*, respectively. The number of amino acids varied from 233 (*AhFRO2.4*) to 738 (*AhFRO7.2*), from 123 (*AdFRO2.3*) to 738 (*AdFRO7*), and from 707 (*AiFRO8*) to 739 (*AiFRO7*) for *AhFRO*, *AdFRO*, and *AiFRO* proteins, respectively. The molecular weight varied from 25.97 kDa (*AhFRO2.4*) to 83.53 kDa (*AhFRO2.2*), from 13.52 kDa (*AdFRO2.3*) to 83.14 kDa (*AdFRO7*), and from 79.36 kDa (*AiFRO8*) to 83.21 kDa (*AiFRO7*) for *AhFRO*, *AdFRO*, and *AiFRO* proteins, respectively. The instability index for most *FRO* proteins was larger than 40, suggesting a low stability in vitro. All *FRO* proteins showed a high aliphatic index (91.87–112.43), implying a high stability over a wide temperature range. The GRAVY of all *FRO* proteins except *AdFRO2.3* is higher than 0, indicating that *FRO*s are hydrophobic proteins. Most of the *FRO* proteins are basic proteins (pI > 7) (Table 1). The number of TMDs for most *FRO* ranged from 8 to 12, while *AhFRO2.4* and *AdFRO2.2* had two TMDs. No TMD was detected in *AdFRO2.3* (Table 1). *FRO2* proteins were predicted to be localized in plasma membranes, while *FRO7* and *FRO8* were localized in chloroplast and mitochondria, respectively (Table 1).

To comprehensively dissect the evolutionary relationship of the *FRO* gene family, a phylogenetic analysis was carried out on 35 *FRO* proteins from *A. hypogaea*, *A. duranensis*, *A. ipaënsis*, and other four plant species (Figure 1). As shown in Figure 1, the *FRO* proteins could be classified into three groups. Group I, which is signed by five *Arabidopsis* AtFROs (AtFRO1–5), includes five *AhFRO*s (*AhFRO2.1/2.2/2.3/2.4/2.5*), three *AdFRO*s (*AdFRO2.1/2.2/2.3*), and one *AiFRO*s (*AiFRO2*) from peanut, *A. duranensis*, and *A. ipaënsis*, respectively. Group II is signed by two *Arabidopsis* AtFROs (AtFRO6/7) and is composed of *AhFRO7.1/7.2*, *AiFRO7*, and *AdFRO7*. Group III consists of AtFRO8, *AhFRO8.1/8.2*, *AiFRO8*, and *AdFRO8*. By contrast, the three *Arachis* species showed closer relationships with another legume species (*M. truncatula*) in terms of *FRO* proteins.

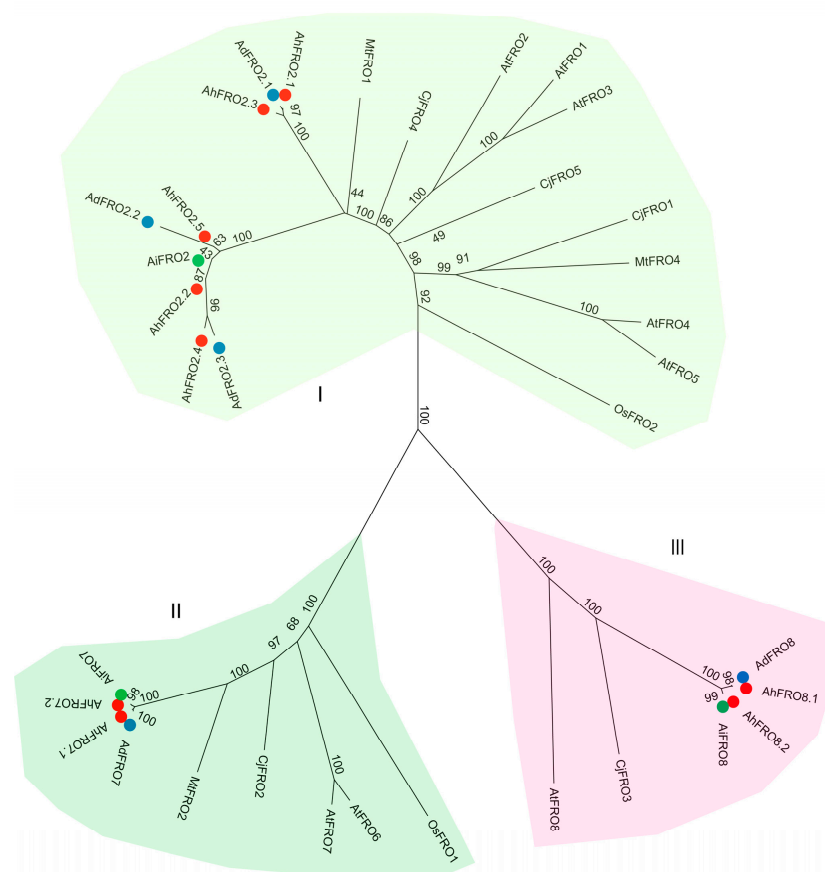


Figure 1. Phylogenetic relationships of FRO proteins in the three *Arachis* species and other plant species. The species involved in the evolutionary tree include *A. hypogaea* (AhFRO), *A. duranensis* (AdFRO), *A. ipaënsis* (AiFRO), *Arabidopsis thaliana* (AtFRO), *Oryza sativa* (OsFRO), *Citrus junos* (CjFRO), and *Medicago truncatula* (MtFRO). The AhFRO, AdFRO, and AiFRO proteins are marked in red, blue, and green colors, respectively.

2.2. Conserved Motifs, Domain Architectures, and Exon–Intron Organization

A total of ten conserved motifs (1–10) were identified in FRO proteins, with the length varying from 21 to 50 (Figure 2A and Table S1). The majority of FRO proteins contained the ten conserved motifs. However, AhFRO2.4, AdFRO2.2, and AdFRO2.3 only contained four, three, and two motifs, respectively. The composition of conserved motifs was similar within phylogenetic groups. All FRO proteins contained the typical domains (Ferric_reduct, FAD_binding_8, and NAD_binding_6) except AhFRO2.4, AdFRO2.2, and AdFRO2.3 in which only the NAD_binding_6 domain was detected (Figure 2B).

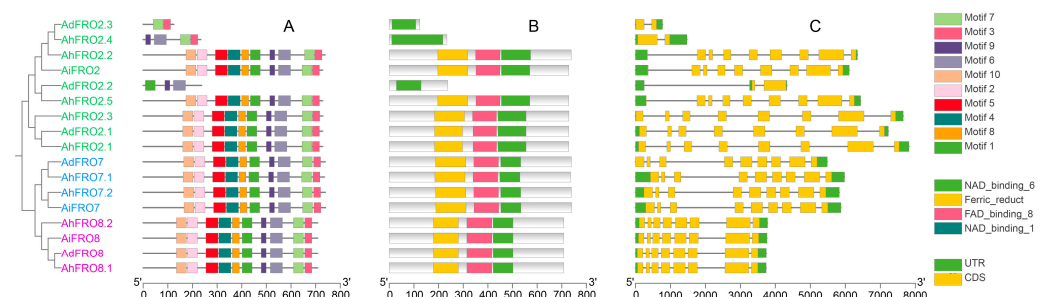


Figure 2. Conserved motifs (A) and domains (B) in FRO proteins and exon–intron organization of FRO genes (C) from the three *Arachis* species. UTR and CDS represent untranslated regions and coding sequences, respectively.

Multiple sequence alignment indicated that all AhFROs have conserved motifs such as C(L/M)AxL, YHxWLG, and HG in the Ferric_reduct domain, LQWH(P/S)F in the FAD_binding domain, and GGxG(I/L)(T/S)PF in the NAD_binding domain (Figure S2). In addition, some conserved motifs including LxxGL, FExFxYxHxLY, LRxxQS, VxIK, EGPY(G/E), and GV(L/F)(V/A)(C/S)GP were also detected in other regions.

To gain insight into the evolution of the *FRO* family in peanut, exon–intron organizations were examined (Figure 2C). *FRO* genes typically contained eight or nine introns, which were separated by seven or eight exons, while only two exons were detected in *AhFRO2.4*, *AdFRO2.2*, and *AdFRO2.3*. The exon–intron organization varied among different phylogenetic groups; however, *FRO* genes belonging to the same group generally had similar structures.

2.3. Gene Duplication of the *FRO* Family

The nine *AhFRO* genes of peanut were distributed in six chromosomes (Ah02, 04, 07, 12, 14, and 17). The sub-genomes A (Ah01–10) and B (Ah11–20) have four and five *AhFRO* genes, respectively (Figure 3A). The number of *AhFRO* genes was the highest in Ah14 (3), followed by Ah04 (2), while only one gene was contained in Ah02, 07, 12, and 17, respectively. Similarly, five *AdFRO* genes of *A. duranensis* were distributed in A02, A04, and A07, while *AiFRO* genes of *A. ipaënsis* were distributed in B02, B04, and B07 (Figure 3B,C).

Synteny analysis revealed that the four *AhFRO* genes of the sub-genome A were crossly collinear with corresponding genes of the sub-genome B, forming four orthologous gene pairs derived from whole-genome duplications (WGDs): *AhFRO2.1/2.3*, *AhFRO2.2/2.4*, *AhFRO7.1/7.2*, and *AhFRO8.1/8.2* (Figure 3A). In addition, segmental duplication also occurred within the two sub-genomes, forming two paralogous gene pairs (*AhFRO2.1/2.2* and *AhFRO2.3/2.4*) (Figure 3A).

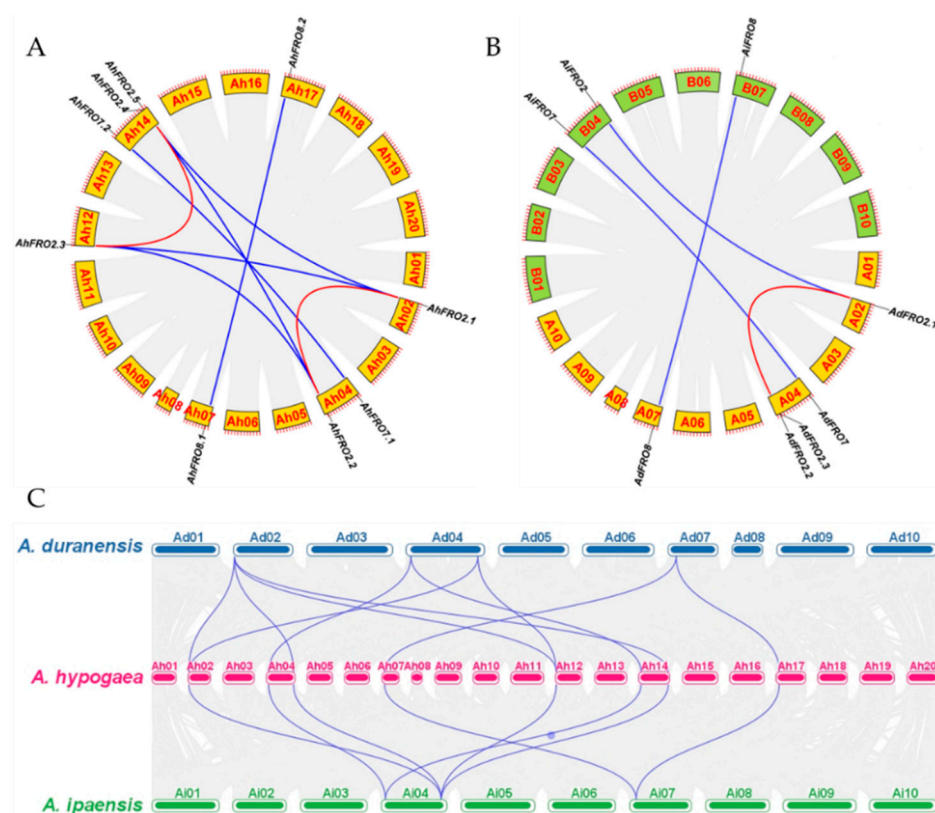


Figure 3. Synteny relationship of *FRO* gene pairs in the three *Arachis* species. (A) Synteny relationship of *AhFRO* gene pairs in *A. hypogaea*. (B) Synteny relationship of *FRO* gene pairs between *A. duranensis* and *A. ipaensis*. (C) Synteny relationship of *FRO* gene pairs among the three *Arachis* species. The red and blue lines represent segmental duplicated genes and syntenic genes, respectively. The gray lines show the collinear blocks of the plant genomes.

To better understand the evolution of the *FRO* gene family, an interspecies synteny analysis was performed on the three *Arachis species*. Three orthologous gene pairs (*AdFRO2.1/AiFRO2*, *AdFRO7/AiFRO7*, and *AdFRO8/AiFRO8*) were identified between *A. duranensis* and *A. ipaënsis*, which is less than that between the two sub-genomes of peanut (Figure 3B). In addition, a block (*AdFRO2.1/AdFRO2.3*) within the genome of *A. duranensis* appears to be WGD/segmental duplication. There were ten and eight collinear blocks between peanut and *A. duranensis* and between peanut and *A. ipaënsis*, respectively (Figure 3C). All *FROs* of *A. duranensis* and *A. ipaënsis* were collinear with those of peanut.

The K_a/K_s ratios of all gene duplication pairs were greatly lower than one (Table 2), indicating that *AhFRO* genes evolved under purifying selection [20]. The divergence time of the four whole genome duplicated gene pairs ranged from 1.21 Mya to 2.38 Mya, which was considerably less than that of the two segmental duplicated gene pairs (43.14 and 44.70 Mya, respectively) (Table 2).

Table 2. K_a/K_s analysis of all gene duplication pairs for *AhFRO* genes.

Gene Pairs	Duplicate Type	K_a ^a	K_s ^b	K_a/K_s ^c	Positive Selection	Divergence Time (Mya)
<i>AhFRO2.1/2.3</i>	Whole-genome	0.011	0.039	0.279	No	2.38
<i>AhFRO2.2/2.4</i>	Whole-genome	0.013	0.020	0.661	No	1.21
<i>AhFRO7.1/7.2</i>	Whole-genome	0.006	0.020	0.302	No	1.21
<i>AhFRO8.1/8.2</i>	Whole-genome	0.011	0.027	0.422	No	1.63
<i>AhFRO2.1/2.2</i>	Segmental	0.209	0.726	0.289	No	44.70
<i>AhFRO2.3/2.4</i>	Segmental	0.203	0.701	0.290	No	43.14

^a The number of nonsynonymous substitutions per nonsynonymous site, ^b the number of synonymous substitutions per synonymous site, ^c K_a/K_s ratios.

2.4. 3D Model Predictions and Multiple Sequence Alignment

To obtain a reasonable theoretical structure of *FROs*, 3D model predictions were performed using the Swiss-Model server (Figure 4 and Table S2). Most of the *FRO2* proteins in peanut and the progenitors were well modeled with the homologous template, 7d3f.1, which is a cryo-EM structure of human DUOX1–DUOX1 in a high-calcium state (Figure 4 and Table S2). All *FRO7* were well modeled with 6wxr.1, the cryoEM structure of mouse DUOX1–DUOX1 complex in the absence of NADPH, while *FRO8* was well modeled with 8gz3.1, the structure of human phagocyte NADPH oxidase in the resting state. Apart from three short sequence proteins (*AhFRO2.4*, *AdFRO2.2*, and *AdFRO2.3*), all *FRO* proteins from peanut and the progenitors share more than 20% sequence identity with their homologous templates, and the GMQE values ranged from 0.29 to 0.43 (Table S2), suggesting a high reliability of 3D model predictions.

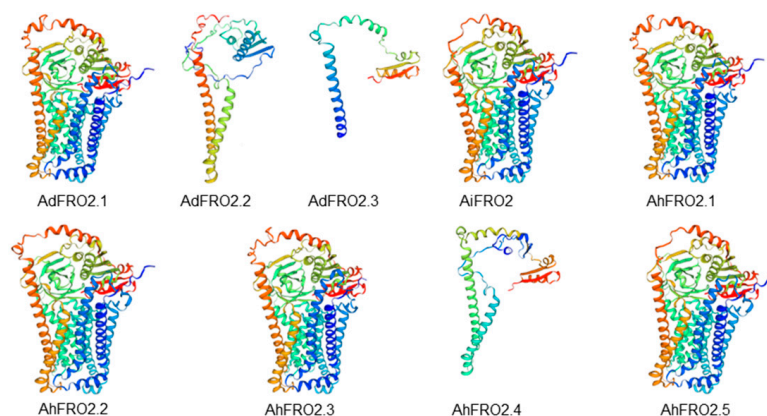


Figure 4. Cont.

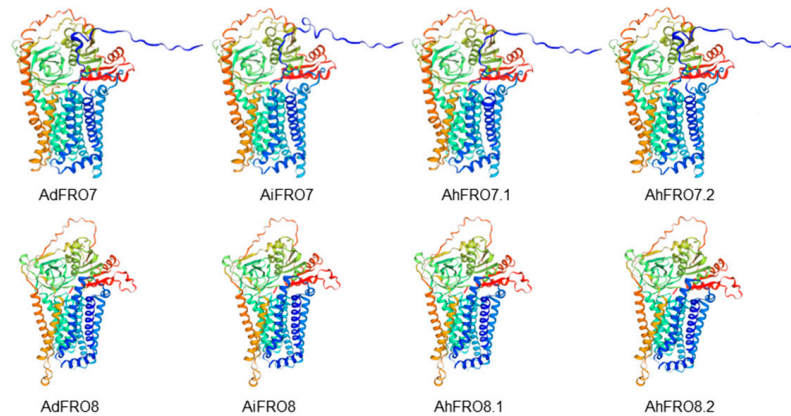


Figure 4. Predicted 3D structure of peanut AhFRO proteins by Swiss-Model. Models were visualized with rainbow colors from N to C terminus.

2.5. The Cis-Regulatory Elements (CREs) of AhFRO Genes in Peanut

A total of 1040 CREs were identified in the promoter region of *AhFRO* genes, and most of them are associated with gene transcription, light response, phytohormone response, and abiotic stress (Table 3). The main light-responsive CREs are TCT-motif, Box 4, ATCT-motif, GT1-motif, G-box, and AT1-motif. The main phytohormone-responsive CREs included ABRE, P-box, and TCA-element. The abiotic stress-responsive CREs are TC-rich repeats, ARE, LTR, and MBS. The promoter of all *AhFRO* genes contained CAAT-box, TATA-box, and TCT-motif; however, the distribution of remaining CREs widely varied among *AhFRO* genes. *AhFRO2.3* contained the most light-responsive CREs, while *AhFRO8.1* had the most phytohormone-responsive elements. *AhFRO2.2* and *AhFRO2.5* have the fewest types of CREs (Table 3).

Table 3. The cis-regulatory elements in the promoter regions of *AhFRO* genes in peanut.

Function	cis-Acting Elements	<i>AhFRO2.1</i>	<i>AhFRO2.2</i>	<i>AhFRO2.3</i>	<i>AhFRO2.4</i>	<i>AhFRO2.5</i>	<i>AhFRO7.1</i>	<i>AhFRO7.2</i>	<i>AhFRO8.1</i>	<i>AhFRO8.2</i>
Gene transcription	CAAT-box	9	20	14	19	12	8	6	13	15
	TATA-box	99	66	151	73	91	106	121	56	52
Light responsive-ness	3-AF1 binding site			1						
	ACE					1				
	AE-box				1					
	AT1-motif					1	3	3	1	
	ATC-motif						1	1		
	ATCT-motif	1	1	1		1				
	Box4	5	6	5		9	2	4	3	11
	chs-CMA1a								2	
	chs-CMA2a								1	
	GA-motif	1		1						
	GATA-motif	2		3	1					
	G-box			1				3	4	5
	GT1-motif	1	2	1			3	3	5	
	I-box	2		2	3					
	MRE			1						
TCCC-motif							1		1	
TCT-motif	1	1	1	2		1	2	3	1	
Phytohormone responsive	ABRE			1			3	3	3	
	CGTCA-motif			1					1	2
	GARE-motif		1			1			1	
	P-box	1	1		1					
	TCA-element					1		1	1	1
	TGACG-motif			1					1	2
	TGA-element						1			
AuxRR-core								1	1	
Abiotic stress responsive	ARE	3	2	4	3				3	8
	LTR			1						
	MBS	1					1			
	TC-rich repeats		1		2			1	2	1
Tissue expression	CAT-box				1		1	1		
	GCN4_motif						1			1

2.6. Tissue-Specific Expression of *AhFRO* Genes in Peanut

To gain an insight into tissue-specific expression, RNA-seq data of the nine *AhFRO*s were used for studying their expression patterns in different tissues and developmental stages (Table S3). As presented in Figure 5, nine *AhFRO* genes were divided into three clusters. Cluster I included *AhFRO7.1* and *AhFRO7.2*, which show high expression and are mainly transcribed in leaves and pistils. Cluster II is composed of four genes with an intermediate level of expression that is preferentially expressed in the developing seeds, roots, vegetative shoot tip, and mainstem leaves. Cluster III consists of *AhFRO2.1*, *AhFRO2.2*, and *AhFRO2.4*, which show low expression and were predominantly expressed in roots.

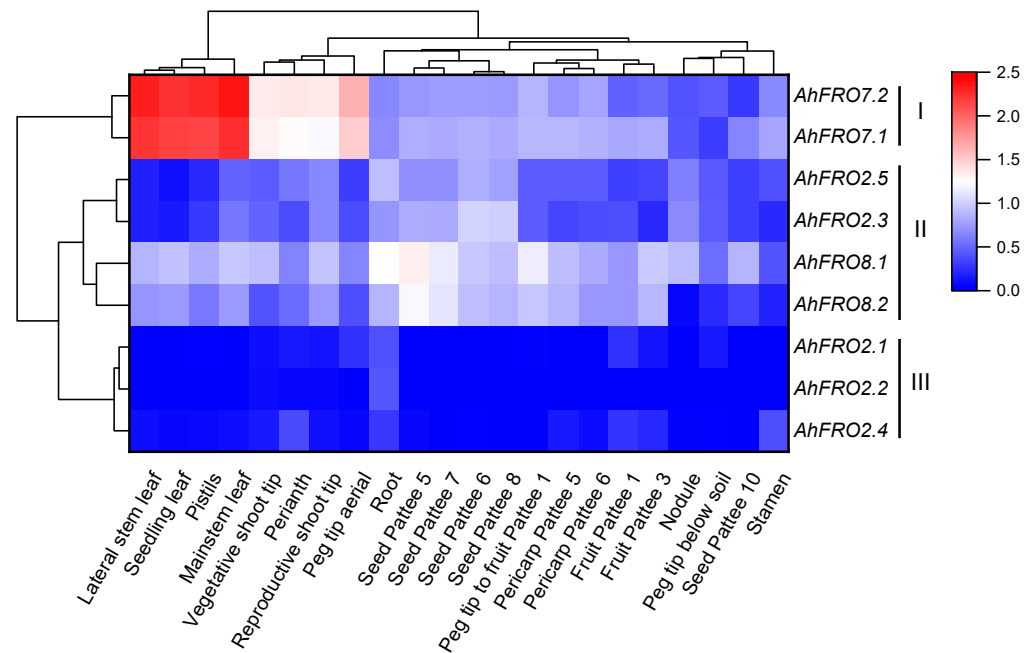


Figure 5. Expression profiles of *AhFRO* genes across the different tissues. Gene expression is expressed in $\lg(\text{TPM} + 1)$. Pattee 1, 3, 5, 6, 7, 8, and 10 represent differential pod developmental stages according to Pattee et al. [21].

2.7. Transcriptional Responses of *AhFRO*s to Fe-Deficiency and Cu Exposure

To elucidate the transcriptional response of *AhFRO*s to Fe deficiency and/or Cu exposure, two contrasting peanut cultivars, Fenghua 1 (Fe deficiency sensitive cultivar) and Silihong (Fe deficiency tolerant cultivar), were used for qRT-PCR analysis. As presented in Figure 6, Cu exposure repressed the expression of *AhFRO7.1/7.2* in the root for both cultivars, while *AhFRO2* genes were not affected. Fe deficiency induced the expression of *AhFRO2.1/2.2/2.3/2.5* but reduced the expression of *AhFRO7.1* in the root for both cultivars. The remaining *AhFRO* genes responded Fe deficiency in a cultivar-specific manner. Cu exposure with Fe deficiency increased the expressions of *AhFRO2.1/2.2/2.4/2.5* but repressed the expression of *AhFRO7.1/7.2* in the root for both cultivars, while the expression of *AhFRO8.1/8.2* was unaffected (Figure 6).

As for the gene expression in leaves, *AhFRO2.2*, *AhFRO7.1/7.2*, and *AhFRO8.1* were repressed by Cu exposure for both cultivars (Figure 7). Fe deficiency induced the expression of *AhFRO2.1/2.2/2.4/2.5* but reduced the expression of *AhFRO8.1/8.2* in the leaves for both cultivars. Cu exposure with Fe deficiency up-regulated the expressions of *AhFRO2.2/2.4/2.5* in the leaves for both cultivars (Figure 7).

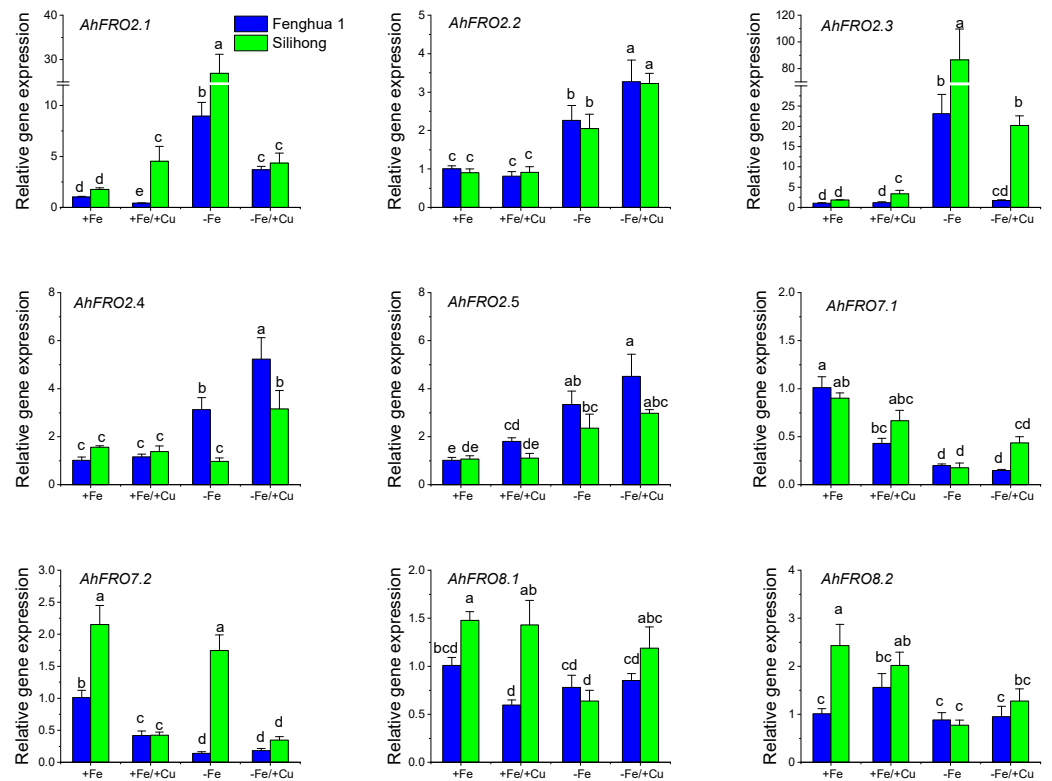


Figure 6. Expression levels of *AhFRO* genes in the root of two peanut cultivars in response to Fe deficiency and/or Cu exposure. Data (means \pm SE, $n = 3$) sharing the same letter(s) above the error bars are not significantly different at the 0.05 level according to the Duncan multiple range test.

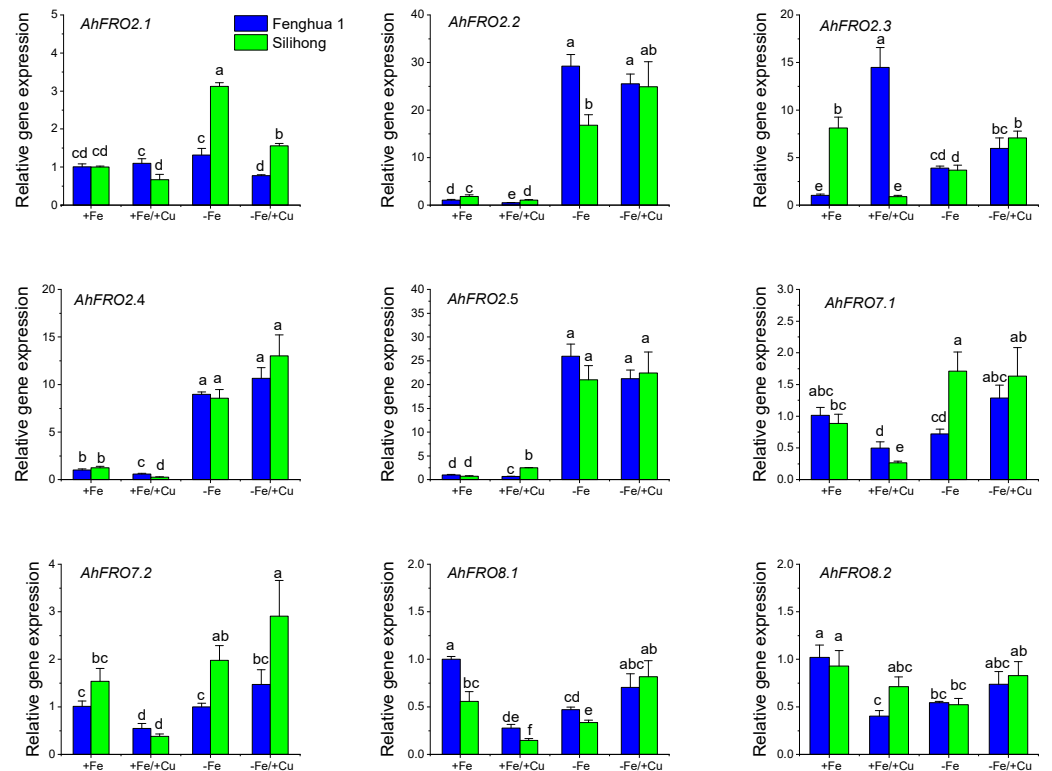


Figure 7. Expression levels of *AhFRO* genes in the leaves of two peanut cultivars in response to Fe deficiency and/or Cu exposure. Data (means \pm SE, $n = 3$) sharing the same letter(s) above the error bars are not significantly different at the 0.05 level based on the Duncan multiple range test.

2.8. The Accumulation and Translocation of Fe and Cu in the Two Peanut Cultivars

The two peanut cultivars differed from each other in Fe accumulation, which was significantly influenced by Fe deficiency and Cu exposure as well as their interactions (Table 4). Under normal conditions (control), Fenghua 1 showed higher Fe concentrations in roots and shoots, and higher total amounts of Fe in plants than Silihong (Table 4). Fe deficiency significantly reduced Fe uptake and accumulation in the peanut plant depending on cultivar and Cu exposure. Cu exposure significantly increased root Fe concentrations in Fe-sufficient peanut plants, resulting in an increase in total amounts of Fe in plants and a reduction of root-to-shoot Fe translocation (Table 4).

Table 4. The accumulation and translocation of Fe and Cu in two peanut cultivars exposed to Fe-deficiency and/or Cu for 14 days.

Cultivars/ Treatments	[Fe] _{root} ^a	[Fe] _{shoot} ^b	Total Fe in Plants	% of Fe in Shoots	[Cu] _{root} ^c	[Cu] _{shoot} ^d	Total Cu in Plants	% of Cu in Shoots
Fenghua 1								
+Fe (control)	1203.2 ± 56.0 ce	159.5 ± 5.2 a	703.4 ± 19.2 c	46.2 ± 2.1 a	19.1 ± 2.0 e	5.5 ± 0.4 f	17.3 ± 1.5 d	65.2 ± 2.3 a
+Fe + Cu	1880.4 ± 48.8 b	109.8 ± 4.3 d	1053.4 ± 41.8 b	28.1 ± 1.4 c	168.5 ± 13.5 d	8.8 ± 0.2 d	91.2 ± 3.5 b	26.0 ± 1.9 c
−Fe	273.2 ± 8.8 f	47.1 ± 1.5 e	165.5 ± 6.9 f	47.0 ± 1.1 a	172.4 ± 6.8 d	16.9 ± 0.4 b	83.3 ± 1.5 bc	33.5 ± 2.0 b
−Fe + Cu	424.8 ± 12.4 e	48.2 ± 0.7 e	238.4 ± 21.6 e	38.1 ± 2.0 b	1742.1 ± 27.6 a	51.6 ± 1.6 a	701.2 ± 58.8 a	13.8 ± 0.6 e
Silihong								
+Fe (control)	1064.4 ± 24.9 d	121.3 ± 2.0 c	569.9 ± 15.9 d	45.1 ± 1.5 a	12.7 ± 1.2 e	3.4 ± 0.1 g	10.8 ± 0.4 d	65.7 ± 2.2 a
+Fe + Cu	2868.4 ± 43.8 a	133.2 ± 4.1 b	1240.5 ± 6.6 a	23.4 ± 0.9 d	192.8 ± 9.9 cd	6.9 ± 0.1 e	78.8 ± 1.8 bc	19.1 ± 0.8 d
−Fe	504.2 ± 48.2 e	44.2 ± 2.5 e	167.1 ± 5.9 f	34.7 ± 1.0 b	199.9 ± 3.3 c	13.4 ± 0.6 c	61.7 ± 5.8 c	28.8 ± 0.7 c
−Fe + Cu	473.9 ± 31.9 e	50.2 ± 3.0 e	275.2 ± 25.8 e	35.7 ± 1.3 b	1649.3 ± 24.8 b	54.4 ± 2.4 a	719.3 ± 19.3 a	14.7 ± 0.4 de
ANOVA (F value)								
Cu	582.2 ***	11.1 **	397.4 ***	131.3 ***	6515.8 ***	752.6 ***	516.9 ***	729.6 ***
Fe	2451.4 ***	1326.4 ***	2038.3 ***	9.3 **	6602.5 ***	1381.0 ***	481.0 ***	369.4 ***
Cultivar (Cv)	109.6 ***	3.0 ns	2.3 ns	23.7 ***	1.3 ns	2.6 ns	0.1 ns	5.4 *
Cu × Fe	478.7 ***	23.9 ***	194.0 ***	58.5 ***	4204.2 ***	525.8 ***	330.7 ***	137.8 ***
Cu × Cv	76.7 ***	52.3 ***	34.9 ***	2.3 ns	4.7 *	4.8 *	0.3 ns	0.1 ns
Fe × Cv	27.8 ***	2.2 ns	0.1 ns	4.5 *	4.0 ns	1.2 ns	0.1 ns	0.3 ns
Cu × Fe × Cv	147.2 ***	38.0 ***	22.4 ***	10.4 **	13.2 **	3.9 ns	0.5 ns	8.6 *

^a Fe concentration in roots, ^b Fe concentration in shoots, ^c Cu concentration in roots, ^d Cu concentration in shoots. Data (means ± SE, $n = 3$) sharing the same letter(s) in the same column are not significantly different at the 0.05 level based on the Duncan multiple range test. * $p < 0.05$, ** $p < 0.01$, *** $p < 0.001$, ns, not significant.

The two peanut cultivars are similar in Cu accumulation and translocation (Table 4). Cu concentrations in roots and shoots and total amounts of Cu in plants were significantly enhanced by Fe deficiency and Cu exposure, while the percentage of Cu in shoots was reduced (Table 4). There are significant Cu × Fe interactions on Cu accumulation and translocation in the two peanut cultivars (Table 4).

2.9. Relationships between AhFRO Genes and Metal Accumulation in Peanut

Pearson's correlation analysis was performed to determine relationships between AhFRO genes and the accumulation and translocation of Fe and Cu. As shown in Table 5, the expression of all AhFRO2 genes was negatively correlated with Fe concentrations in roots ($p < 0.05$) and shoots ($p < 0.01$) as well as the total Fe in plants ($p < 0.05$). In contrast, AhFRO7.1 and AhFRO8.2 were observed to positively correlate with Fe accumulation ($p < 0.05$). Cu accumulation in peanut plants was positively correlated with the expression of AhFRO2.2/2.4/2.5 ($p < 0.01$) but negatively correlated with the expression of AhFRO7.1/7.2 ($p < 0.05$). The percentage of Cu in shoots was negatively related to the expression of FRO2.2/2.5 ($p < 0.01$) but positively correlated with the expression of AhFRO7.1/7.2 ($p < 0.01$). No significant correlation was found between AhFRO genes and Fe translocation (Table 5).

Table 5. Pearson’s correlation analysis (r value, $n = 24$) of metal accumulation and the expression of *AhFRO* genes in the roots and leaves of Fenghua 1 and Silihong.

Gene Expression	[Fe] _{root} ^a	[Fe] _{shoot} ^b	Total Fe in Plants	% of Fe in Shoots	[Cu] _{root} ^c	[Cu] _{shoot} ^d	Total Cu in Plants	% of Cu in Shoots
Roots								
<i>AhFRO2.1</i>	−0.345	−0.526 **	−0.476 *	−0.059	−0.113	−0.034	−0.144	−0.192
<i>AhFRO2.2</i>	−0.678 **	−0.773 **	−0.714 **	0.173	0.794 **	0.843 **	0.772 **	−0.550 **
<i>AhFRO2.3</i>	−0.380	−0.519 **	−0.481 *	−0.038	−0.084	0.003	−0.103	−0.161
<i>AhFRO2.4</i>	−0.488 *	−0.567 **	−0.500 *	0.199	0.748 **	0.763 **	0.711 **	−0.450 *
<i>AhFRO2.5</i>	−0.603 **	−0.755 **	−0.620 **	0.164	0.660 **	0.702 **	0.624 **	−0.546 **
<i>AhFRO7.1</i>	0.451 *	0.856 **	0.521 **	0.146	−0.437 *	−0.497 *	−0.415 *	0.713 **
<i>AhFRO7.2</i>	−0.071	0.222	−0.079	0.255	−0.461 *	−0.477 *	−0.471 *	0.649 **
<i>AhFRO8.1</i>	0.301	0.345	0.269	−0.013	−0.013	−0.058	−0.020	0.252
<i>AhFRO8.2</i>	0.511 *	0.452 *	0.515 **	−0.203	−0.247	−0.312	−0.253	0.273
Leaves								
<i>AhFRO2.1</i>	−0.405 *	−0.495 *	−0.488 *	−0.050	−0.072	0.008	−0.087	−0.108
<i>AhFRO2.2</i>	−0.754 **	−0.865 **	−0.800 **	0.256	0.618 **	0.707 **	0.622 **	−0.498 *
<i>AhFRO2.3</i>	−0.017	−0.129	0.114	−0.212	0.115	0.103	0.140	−0.113
<i>AhFRO2.4</i>	−0.762 **	−0.868 **	−0.809 **	0.184	0.735 **	0.812 **	0.742 **	−0.530 **
<i>AhFRO2.5</i>	−0.734 **	−0.889 **	−0.806 **	0.193	0.548 **	0.646 **	0.547 **	−0.518 **
<i>AhFRO7.1</i>	−0.639 **	−0.492 *	−0.647 **	0.257	0.440 *	0.473 *	0.440 *	−0.107
<i>AhFRO7.2</i>	−0.585 **	−0.486 *	−0.591 **	0.238	0.506 *	0.536 **	0.525 **	−0.130
<i>AhFRO8.1</i>	−0.474 *	0.053	−0.372	0.595 **	0.350	0.354	0.365	0.325
<i>AhFRO8.2</i>	−0.031	0.357	0.000	0.386	0.086	0.031	0.100	0.452 *

^a Fe concentration in roots, ^b Fe concentration in shoots, ^c Cu concentration in roots, ^d Cu concentration in shoots, * $p < 0.05$, ** $p < 0.01$.

3. Discussion

FRO members have been demonstrated to play crucial roles in the homeostasis of Fe and Cu [9]. However, there has been little work on genome-wide identification of the FRO family in plants. In this study, we identified nine, four, and three FRO genes in peanut, *A. duranensis*, and *A. ipaensis*, respectively (Table 1). The number of *AhFRO* genes in peanut is higher than that in most reported plant species [9,12]. The same phenomenon has been reported in other gene families of peanut [22–25]. Peanut, as an allotetraploid species derived from the hybridization of diploid ancestral species, *A. duranensis* (AA) and *A. ipaensis* (BB) [19], has experienced at least three rounds of WGD events [26]. Our results indicated that eight out of nine *AhFRO* genes have experienced WGD events. Moreover, two paralogous gene pairs (*AhFRO2.1/2.2* and *AhFRO2.3/2.4*) were found to be segmental duplications. Expectedly, the divergence time indicates that segmental duplication events (43.14–44.70 Mya) of *AhFRO* genes occurred dramatically earlier than WGD (1.21–2.38 Mya) (Table 2). It is likely that WGD/segmental duplication contributes to the expansion of the *AhFRO* gene family in peanut.

Gene duplication is a major source of novel genes that contribute to the acquirement of novel functions [27]. However, it results in functional redundancy [28] and, consequently, most duplicated genes quickly pseudogenize and get lost [29]. In the current study, we found that the number of FRO genes differed between the two sub-genomes of peanut and between *A. duranensis* and *A. ipaensis*, which suggests an asymmetrical evolution in the family. Synteny analysis revealed that the orthologs of *AhFRO2.5* and *AhFRO2.3* have been lost in the genome of *A. ipaensis* after allopolyploidization (Figure 3). Likewise, an ortholog of *AdFRO2.3* has been lost in the sub-genome A of peanut. These results, which are in agreement with our previous study [25], confirmed that gene loss is easier in *A. ipaensis* than *A. duranensis*. The number of *AhFRO* genes in peanut is greater than the sum of the two ancestors, suggesting that heteropolyploid is more capable of avoiding gene loss than diploid.

Another approach for avoiding gene loss of duplicated genes is the reduction of their expression compared to the ancestral gene [28]. In the present study, three *AhFRO2* genes showed low expression levels in all tissues of peanut (cv. Tifrunner) under normal conditions (Figure 5). The results concurred with previous studies [25,28], suggesting that the reduction of gene expression might be beneficial for the maintenance of multiple duplicated genes and avoidance of functional redundancy.

Surviving duplicated genes would be subject to purifying selection, which could lead to divergence in both the coding and regulatory regions [30]. At the coding regions, *AhFRO2.4* from peanut and *AdFRO2.2* and *AdFRO2.3* from *A. duranensis* only have two exons, while the remaining *FRO2* genes contained eight exons. Gene/protein structures indicate that these genes appear to derive from continuous gene shortening during evolution, which may cause neofunctionalization or pseudogenization. The inducible gene expression by Fe-deficiency confirms that *AhFRO2.4* still has a function in the Fe-deficient response of peanut roots and leaves.

At the regulatory regions, CREs play essential roles in regulating gene expression through interacting with transcription factors and RNA polymerase [22]. Our results show that, although all duplicated genes of *FRO7*, *FRO8*, and some of *FRO2* (i.e., *AhFRO2.1/2.3*) share a similar exon–intron organization, none of them have similar CREs. The promoter of *AhFRO7.1* specifically contains TCCC-motif, LTR, and GCN4_motif, while that of *AhFRO7.2* specifically contains TCA-element, MBS, and TC-rich repeats. Similarly, the promoter of *AhFRO8.1* specifically contains AT1-motif, chs-CMA1a, chs-CMA2a, and GARE-motif, while that of *AhFRO8.2* specifically contains MRE and GCN4_motif. The differential CREs in promoters imply a divergence of transcriptional regulation between the duplicated genes.

Apart from the three short sequence proteins (*AhFRO2.4*, *AdFRO2.2*, and *AdFRO2.3*), all *FROs* contained the typical domains: Ferric_reduct, FAD_binding_8, and NAD_binding_6 (Figure 2B). Ferric_reduct domain is a ferric reductase-like transmembrane component that can transfer electrons from extracellular ferric ions to generate the reduced form of ferrous ions for transporting across the plasma membrane by specific iron transporters [12,31]. NAD- and FAD-binding domains participate in membrane electron transfer from intracellular NADPH and FAD to extracellular oxygen for superoxide production [11]. Consistent with gene structures, *AhFRO2.4*, *AdFRO2.2*, and *AdFRO2.3* only contain the NAD_binding_6 domain, indicating a distinct physiological function from other homologous proteins.

AhFRO proteins were well modeled with three kinds of 3D model templates such as 6wxr.1, 8gz3.1, and 7d3f.1 (Table S2). The best template of *FRO2* for a 3D model is 7d3f.1, a cryo-EM structure of human DUOX1–DUOX1 in a high-calcium state [32]. The best template of *FRO7* is 6wxr.1, a cryo-EM structure of mouse DUOX1–DUOX1 complex in the absence of NADPH [33]. DUOX1 is an NADPH oxidase family member that catalyzes the production of hydrogen peroxide by transferring electrons from intracellular NADPH to extracellular oxygen [32,33]. *FRO8* is well modeled with 8gz3.1, the structure of human phagocyte NADPH oxidase in the resting state [34]. Phagocyte NADPH oxidase membrane-bound redox enzymes transfer electrons from intracellular NADPH to extracellular oxygen for producing superoxide anions [34]. Structural analysis indicates that *AhFROs* have redox activity and might reduce metal ions in different pathways.

The phylogenetic tree revealed that *FRO* members are grouped into three groups (I, II, and III), which is consistent with previous results [9,12]. Group I is composed of five paralogs of *AhFRO2* (*AhFRO2.1–2.5*), which exhibited considerable differences in the sequence and gene/protein structure. *AhFRO2.4* is a short sequence gene encoding 233 aa, with two TMDs, while other members contained ten TMDs. *AhFRO2* is closely related to *AtFRO1–3* from *Arabidopsis*. *AtFRO2* is responsible for the reduction of solubilized Fe^{3+} to Fe^{2+} at the root surface in *Arabidopsis*, where Fe^{2+} is then transported into the cytoplasm via IRT1 in the root plasma membrane [10,13]. *AtFRO3* localizes to mitochondrial membranes and might serve an analogous function in the mitochondrial iron homeostasis [16,17]. In this study, *AhFRO2* proteins were predicted to be localized in plasma membranes, and

most of *AhFRO2* genes were predominantly expressed in roots. Moreover, the expression of *AhFRO2* genes was strongly induced by Fe deficiency in both the roots and leaves of peanut seedlings. Similar results have been extensively reported in *AtFRO2* and *AtFRO3* of *Arabidopsis* [35,36]. The expression of *AhFRO2* genes in roots was significantly correlated with Fe concentrations in roots and shoots as well as the total Fe in plants, suggesting that *AhFRO2* genes might be involved in the reduction of Fe in peanut roots.

Group II contained two paralogs of *AhFRO7* (*AhFRO7.1/7.2*), which resulted from WGD events. The two paralogs are very similar in their sequence, physicochemical properties, and gene/protein structure, suggesting the same role in peanut. Phylogenetic analysis indicates that *AhFRO7* is closely clustered with *AtFRO6/7* from *Arabidopsis* and *OsFRO1* from rice. *AtFRO6* has been proven to mediate the reduction of Fe^{3+} to Fe^{2+} at the plasma membrane of leaf cells [9,14], while *AtFRO7* plays a role in chloroplast iron acquisition by reducing Fe^{3+} to Fe^{2+} [15,16]. In the current study, *AhFRO7* proteins were predicted to be localized in chloroplast, which is consistent with *AtFRO7* in *Arabidopsis* [15,16]. Concurrent with Mukherjee et al. [9], who found that *AtFRO6* and *AtFRO7* show high expression in all the green parts of *Arabidopsis* plants, RNA-seq data showed that *AhFRO7.1/7.2* are highly expressed in leaves and pistils. The findings indicate a possible role for *AhFRO7.1/7.2* in regulating chloroplast iron acquisition. Additionally, it is thought that Fe is mainly stored in plastids of plant cells as ferritin [9]. Thus, the repression of *AhFRO7.1/7.2* expression in the roots under Fe deficiency might contribute to Fe translocation to leaves by reducing Fe storage in the plastids of root cells. This is illustrated by the positive correlation between the expression of *AhFRO7.1/7.2* and shoot Fe concentration. In contrast to roots, the expression of *AhFRO7.1/7.2* was induced or unaffected in the leaves. This could maintain or improve Fe reduction ability for importing into chloroplasts in leaves.

Group III included two paralogs of *AhFRO8* derived from WGD, which share the same physicochemical properties and gene/protein structure. Phylogenetic analysis indicates that *AhFRO8* is closely clustered with *AtFRO8* from *Arabidopsis*. Similar to *AtFRO8* [16,17], *AhFRO8.1/8.2* were predicted to localize to mitochondrial membranes. Unlike *AtFRO8* which is highly expressed in *Arabidopsis* shoots [9], our results show that *AhFRO8.1/8.2* are primarily expressed in seeds and roots (*AhFRO8.1*) of peanut. Previous studies showed that *AtFRO8* is not regulated by Fe availability [9]. However, our results show that Fe deficiency reduces the expression of *AhFRO8.1/8.2* in the roots of Silihong and in the leaves of both cultivars. In addition, the expression of *AhFRO8.1/8.2* in roots was observed to be positively correlated with shoot Fe concentrations. Although the functions of *FRO8* are yet uncharacterized even in *Arabidopsis*, our data implies *AhFRO8.1/8.2* might be involved in mitochondrial iron homeostasis. The reduction of *AhFRO8.1/8.2* under Fe deficiency could reduce Fe storage in the mitochondria, leading to more Fe allocation to chloroplasts.

FRO genes are also assumed to be involved in copper reduction [9,10]. *Arabidopsis AtFRO2* has been shown to take a role in the reduction of Cu^{2+} to Cu^{+} at the root surface [10]. Although *AhFRO2* genes are not regulated by Cu in peanut roots, down-regulation of *AhFRO2.2/2.4* was observed in the leaves under Cu exposure. Moreover, the expression of *AhFRO2.2/2.4/2.5* positively correlated with Cu concentrations in roots and shoots as well as total Cu in plants, indicating a possible role in Cu reduction at the plasma membrane for the uptake of Cu into cells. In addition, we found that excess Cu considerably represses the expression of *AhFRO7.1/7.2* in the roots and leaves for both cultivars. The expression of *AhFRO7.1/7.2* in the roots negatively correlated with Cu concentrations in roots and shoots but positively correlated with root-to-shoot Cu translocation in peanut plants. These data suggest that *AhFRO7.1/7.2* might be involved in Cu homeostasis in peanut plants.

Interestingly, Cu and Fe could interact with each other in their accumulation and translocation in the two peanut cultivars (Table 4). Consistent with previous studies [37], we found that Fe deficiency significantly enhanced Cu concentrations in roots and shoots, and total amounts of Cu in plants, but reduced the percentage of Cu in shoots. As Fe deficiency can induce the expression of *AhFRO2.2/2.4/2.5* in roots, which positively correlated with Cu concentrations in roots and shoots as well as total Cu in plants, we assumed that

AhFRO2.2/2.4/2.5 might be responsible for higher Cu accumulation in Fe-deficient peanut plants. Similarly, the reduction of *AhFRO7.1/7.2* expression under Fe deficiency appears to decrease Cu storage in plastids of root cells and, consequently, contribute to a higher capability of Cu translocation from roots to shoots. Although Cu exposure significantly increased root Fe concentrations in Fe-sufficient peanut plants, none of the *AhFRO* genes could well explain the phenomenon.

As for the two cultivars, Silihong (Fe-deficiency tolerant cultivar) showed higher expressions of *AhFRO2.1/2.3* than Fenghua 1 (Fe-deficiency sensitive cultivar) under Fe-deficiency. Higher expressions of *AhFRO2.1/2.3* indicate a higher capacity for the reduction of Fe^{3+} to Fe^{2+} or Cu^{2+} to Cu^{+} . This is in accordance with the higher concentrations of Fe and Cu in the root of Silihong under Fe deficiency compared with Fenghua 1. It is likely that higher expressions of *AhFRO2.1/2.3* contribute to Fe-deficiency tolerance in Silihong.

4. Materials and Methods

4.1. Identification of FRO Proteins in the Three *Arachis* Species

Protein sequences of *Arabidopsis* AtFROs (AtFRO1–8) were retrieved from a phytozome database (<https://phytozome-next.jgi.doe.gov/>, accessed on 2 May 2022). Using these sequences as queries, BLASTp was carried out against protein databases of *A. hypogaea* cv. Tifrunner, *A. duranensis*, and *A. ipaënsis*, which was retrieved from NCBI (<https://github.com/ncbi>, accessed on 10 May 2022). Non-redundant putative candidates were examined for the presence of typical conserved domains of FROs, Ferric_reduct (PF01794), FAD_binding_8 (PF08022), and NAD_binding_6 (PF08030), using the hmmscan tool (<https://www.ebi.ac.uk/Tools/hmmer/search/hmmscan>, accessed on 12 June 2023). Sequences containing conserved domains were used for the ClustalW alignment and phylogenetic analysis using the MEGA-X program (v. 10.2.6) together with the eight AtFROs. The phylogenetic trees were built using the neighbor-joining (NJ) method based on the Poisson model with 1000 bootstrap replicates. The proteins clustered with AtFROs were assigned as putative FRO proteins.

4.2. Physicochemical and Structural Characteristics of FRO Proteins

Physicochemical characteristics of FRO proteins were analyzed using the ProtParam tool (<https://web.expasy.org/protparam/>, accessed on 23 June 2023) [38]. The transmembrane domains (TMDs) were estimated by TOPCONS (<http://topcons.net/>, accessed on 18 June 2023) [39]. Subcellular targeting sites for FRO proteins were predicted using ProtComp v. 9.0 (<http://www.softberry.com/berry.phtml?topic=protcomppl&group=programs&subgroup=proloc>, accessed on 28 July 2023). The conserved domain of FRO proteins was detected by the Pfam tool (<http://pfam.xfam.org/search#tabview=tab1>, accessed on 21 July 2023) [40]. Conserved motif annotations were obtained from the MEME v. 5.3.3 (<https://meme-suite.org/meme/tools/meme>, accessed on 28 July 2023) [41]. Homology-modeled 3D structures of FRO proteins were predicted using the Swiss-Model (<https://swissmodel.expasy.org/>, accessed on 24 September 2023) [42].

4.3. Exon–intron Organization, Duplication, and Ka/Ks of FRO Genes

The exon–intron organization of *FRO* genes was identified using the GSDS (v. 2.0) (<http://gsds.gao-lab.org/>, accessed on 11 June 2023) [43]. One Step MCScanX integrated into the TBtools software (v. 2.034) was used for detecting the synteny relationship and duplication pattern of *FRO* genes [44]. Diagrams of exon–intron organization and gene duplication events were drawn using TBtools software [44]. Ka/Ks ratios were estimated by the simple Ka/Ks calculator (NJ) integrated into the TBtools software (v. 2.034) [44]. Based on Ks values, the divergence time of the duplication event was calculated with the equation $T = Ks/2\lambda$, where λ represents the neutral substitution rate that is estimated at 8.12×10^{-9} for peanut [18]. The CREs in promoter sequences (upstream 2.0 kb) of *AhFRO* genes were predicted by PlantCARE software (<http://bioinformatics.psb.ugent.be/webtools/plantcare/html/>, accessed on 1 January 2023).

4.4. Tissue-specific Expression Profiles of *AhFRO* Genes in Peanut

RNA-seq data of 22 different tissues in peanut (cv. Tifrunner) were obtained from PeanutBase (<https://www.peanutbase.org/>, accessed on 15 June 2022) [21]. After being transformed from read counts, TPMs (Transcripts Per Kilobase of exon model per Million mapped reads) were used as $\lg(\text{TPM} + 1)$ for constructing a heatmap diagram by Origin 2021 (v 9.8.0.200, OriginLab Corp., Northampton, MA, USA).

4.5. Plant Growth, Treatment, Metal Determination, and RT-qPCR Analysis

Two contrasting peanut cultivars, Fenghua 1 (Fe deficiency sensitive cultivar) and Silihong (Fe deficiency tolerant cultivar), were used for hydroponic experiments [37]. After the surface was sterilized with 5% sodium hypochlorite solution, seeds were rinsed in deionized water for 24 h at room temperature and then sown in sand for germination. Three-day-old seedlings with uniform sizes were transplanted into polyethylene pots for hydroponic culture. The culture conditions and nutrient solutions were followed as described previously by Lu et al. [45]. Ten-day-old seedlings were exposed to 0 or 10 μM CuSO_4 under Fe-sufficient (+Fe, 50 μM Fe-EDTA) or Fe-deficient (−Fe, 0 μM Fe-EDTA) conditions, respectively. Each treatment per cultivar was repeated three times (biological replicates) with three plants per replication. Nutrient solutions were renewed twice a week during the growing period. After 14 days of treatment, plants were harvested for metal determination and RT-qPCR analysis.

The harvested roots were rinsed with 20 mM Na_2EDTA for 15 min to remove the surface-bound metal ions and then oven-dried together with shoots. After being weighed and ground, tissue powders were digested with $\text{HNO}_3\text{--HClO}_4$ (3:1, *v/v*). Cu and Fe concentrations in the samples were determined by flame atomic absorbance spectrometry (WFX-110, Beijing Rayleigh Analytical Instrument Company, Beijing, China). The total Fe/Cu in plants and the percentage of Fe/Cu in shoots were calculated using the equations reported by Liu et al. [46].

Frozen tissues were used for total RNA extraction, cDNA strand synthesis, and RT-qPCR analysis, which were strictly followed according to the methods described by Tan et al. [25]. The relative mRNA abundance was normalized using the endogenous reference gene (*60S*, NCBI Entrez gene ID:112697914). The primers of *AhFROs* and *60S* are listed in Table S4. The relative gene expression was calculated with three biological replicates using the $2^{-\Delta\Delta\text{CT}}$ method [47]. Each biological replication was technically replicated three times.

4.6. Statistical Analysis

1 and Duncan's Multiple Range Test ($p < 0.05$) was used for detecting differences among group means. Pearson's correlation analysis was used to determine the relationship between gene expression and Fe/Cu accumulation. All statistical analyses were conducted using IBM SPSS Statistics v.22 (IBM, New York, NY, USA).

5. Conclusions

A total of nine, four, and three *FRO* genes were identified in peanut, *A. duranensis*, and *A. ipaensis*, respectively, which were divided into three groups (I to III). Most of the *AhFRO* genes underwent WGD/segmental duplication, leading to the expansion of the *AhFRO* gene family. Clustered members generally share similar gene/protein structures. However, structural or CRE divergences and reduced expression existed in *AhFRO* genes, which may be beneficial for the maintenance of duplicate genes. *AhFRO2* and *AhFRO7* genes might be involved in the reduction of Fe/Cu in plasma membranes and chloroplast (or plastids in root cells), while *AhFRO8* genes appear to confer Fe reduction in the mitochondria. Fe deficiency-induced Cu accumulation in both cultivars, which might be associated with *AhFRO2.2/2.4/2.5* and *FRO7.1/7.2*. Our findings provide a basis for further functional characterization of *AhFRO* genes and shed new light on the possible roles of the *AhFRO* family in the Fe/Cu interaction in plants.

Supplementary Materials: The following supporting information can be downloaded at: <https://www.mdpi.com/article/10.3390/plants13030418/s1>, Figure S1: Screening FROs from candidate sequences identified by a BLASTp search against the peanut genome using phylogenetic analysis with AtFROs from *Arabidopsis*; Figure S2: Complete multiple sequence alignment of the FRO proteins from peanut, *A. duranensis*, and *A. ipaensis* with AtFRO2 as a reference; Table S1: Analysis of the ten conserved motifs of AhFRO proteins in peanut; Table S2: The best templates of peanut AhFRO proteins selected from the Swiss-Model template library for building 3D structure models; Table S3: Expression profiles (TPM) of *AhFRO* genes in different tissues of peanut; Table S4: Primers of peanut *AhFRO* genes for RT-qPCR analysis.

Author Contributions: Conceptualization, J.G. and G.S.; methodology, G.S.; validation, J.G., Z.Z. and G.S.; formal analysis, J.G. and G.S.; investigation, J.G. and G.S.; resources, G.S.; data curation, J.G. and G.S.; writing—original draft preparation, J.G., Z.Z. and G.S.; writing—review and editing, J.G. and G.S.; supervision, G.S.; project administration, G.S.; funding acquisition, Z.Z. and G.S. All authors have read and agreed to the published version of the manuscript.

Funding: This work was supported by grants from the Natural Science Foundation of Anhui Province (Grant Number 2108085MC83).

Data Availability Statement: Data are contained within the article.

Conflicts of Interest: The authors declare no conflicts of interest.

References

- Marschner, H. *Mineral Nutrition of Higher Plants*, 2nd ed.; Academic Press: London, UK, 1995; pp. 6–78.
- Therby-Vale, R.; Lacombe, B.; Rhee, S.Y.; Nussaume, L.; Rouached, H. Mineral nutrient signaling controls photosynthesis: Focus on iron deficiency-induced chlorosis. *Trends Plant Sci.* **2022**, *27*, 502–509. [[CrossRef](#)]
- Vigani, G. Discovering the role of mitochondria in the iron deficiency-induced metabolic responses of plants. *J. Plant Physiol.* **2012**, *169*, 1–11. [[CrossRef](#)]
- Wu, L.; Ueda, Y.; Lai, S.-K.; Frei, M. Shoot tolerance mechanisms to iron toxicity in rice (*Oryza sativa* L.). *Plant Cell Environ.* **2017**, *40*, 570–584. [[CrossRef](#)]
- Li, M.; Watanabe, S.; Gao, F.; Dubos, C. Iron nutrition in plants: Towards a new paradigm? *Plants* **2023**, *12*, 384. [[CrossRef](#)] [[PubMed](#)]
- Chen, Y.; Barak, P. Iron Nutrition of Plants in Calcareous Soils. In *Advances in Agronomy*; Brady, N.C., Ed.; Academic Press: Cambridge, MA, USA, 1982; Volume 35, pp. 217–240.
- World Health Organization. Conclusions and recommendations of the WHO Consultation on prevention and control of iron deficiency in infants and young children in malaria-endemic areas. *Food Nutr. Bull.* **2007**, *28*, S621–S627. [[CrossRef](#)]
- Kobayashi, T.; Nishizawa, N.K. Iron sensors and signals in response to iron deficiency. *Plant Sci.* **2014**, *224*, 36–43. [[CrossRef](#)] [[PubMed](#)]
- Mukherjee, I.; Campbell, N.H.; Ash, J.S.; Connolly, E.L. Expression profiling of the *Arabidopsis* ferric chelate reductase (FRO) gene family reveals differential regulation by iron and copper. *Planta* **2006**, *223*, 1178–1190. [[CrossRef](#)]
- Robinson, N.J.; Procter, C.M.; Connolly, E.L.; Guerinot, M.L. A ferric-chelate reductase for iron uptake from soils. *Nature* **1999**, *397*, 694–697. [[CrossRef](#)] [[PubMed](#)]
- Schagerlöff, U.; Wilson, G.; Hebert, H.; Al-Karadaghi, S.; Hägerhäll, C. Transmembrane topology of FRO₂, a ferric chelate reductase from *Arabidopsis thaliana*. *Plant Mol. Biol.* **2006**, *62*, 215–221. [[CrossRef](#)] [[PubMed](#)]
- Muhammad, I.; Jing, X.-Q.; Shalmani, A.; Ali, M.; Yi, S.; Gan, P.-F.; Li, W.-Q.; Liu, W.-T.; Chen, K.-M. Comparative in silico analysis of ferric reduction oxidase (FRO) genes expression patterns in response to abiotic stresses, metal and hormone applications. *Molecules* **2018**, *23*, 1163. [[CrossRef](#)]
- Brumbarova, T.; Bauer, P.; Ivanov, R. Molecular mechanisms governing *Arabidopsis* iron uptake. *Trends Plant Sci.* **2015**, *20*, 124–133. [[CrossRef](#)]
- Li, L.-Y.; Cai, Q.-Y.; Yu, D.-S.; Guo, C.-H. Overexpression of AtFRO6 in transgenic tobacco enhances ferric chelate reductase activity in leaves and increases tolerance to iron-deficiency chlorosis. *Mol. Biol. Rep.* **2011**, *38*, 3605–3613. [[CrossRef](#)] [[PubMed](#)]
- Jeong, J.; Cohu, C.; Kerkeb, L.; Pilon, M.; Connolly, E.L.; Guerinot, M.L. Chloroplast Fe(III) chelate reductase activity is essential for seedling viability under iron limiting conditions. *Proc. Natl. Acad. Sci. USA* **2008**, *105*, 10619–10624. [[CrossRef](#)]
- Jeong, J.; Connolly, E.L. Iron uptake mechanisms in plants: Functions of the FRO family of ferric reductases. *Plant Sci.* **2009**, *176*, 709–714. [[CrossRef](#)]
- Jain, A.; Wilson, G.T.; Connolly, E.L. The diverse roles of FRO family metallo-reductases in iron and copper homeostasis. *Front. Plant Sci.* **2014**, *5*, 100. [[CrossRef](#)] [[PubMed](#)]

18. Bertoli, D.J.; Cannon, S.B.; Froenicke, L.; Huang, G.; Farmer, A.D.; Cannon, E.K.S.; Liu, X.; Gao, D.; Clevenger, J.; Dash, S.; et al. The genome sequences of *Arachis duranensis* and *Arachis ipaensis*, the diploid ancestors of cultivated peanut. *Nat. Genet.* **2016**, *48*, 438–446. [[CrossRef](#)] [[PubMed](#)]
19. Bertoli, D.J.; Jenkins, J.; Clevenger, J.; Dudchenko, O.; Gao, D.; Seijo, G.; Leal-Bertoli, S.C.M.; Ren, L.; Farmer, A.D.; Pandey, M.K.; et al. The genome sequence of segmental allotetraploid peanut *Arachis hypogaea*. *Nat. Genet.* **2019**, *51*, 877–884. [[CrossRef](#)]
20. Hurst, L.D. The Ka/Ks ratio: Diagnosing the form of sequence evolution. *Trends Genet.* **2002**, *18*, 486–487. [[CrossRef](#)]
21. Clevenger, J.; Chu, Y.; Scheffler, B.; Ozias-Akins, P. A developmental transcriptome map for allotetraploid *Arachis hypogaea*. *Front. Plant Sci.* **2016**, *7*, 1446. [[CrossRef](#)]
22. Wang, X.; Wang, C.; Zhang, Z.; Shi, G. Genome-wide identification of metal tolerance protein genes in peanut: Differential expression in the root of two contrasting cultivars under metal stresses. *Front. Plant Sci.* **2022**, *13*, 791200. [[CrossRef](#)]
23. Zhang, Z.; Chen, N.; Zhang, Z.; Shi, G. Genome-wide identification and expression profile reveal potential roles of peanut ZIP family genes in zinc/iron-deficiency tolerance. *Plants* **2022**, *11*, 786. [[CrossRef](#)]
24. Wang, C.; Wang, X.; Li, J.; Guan, J.; Tan, Z.; Zhang, Z.; Shi, G. Genome-wide identification and transcript analysis reveal potential roles of oligopeptide transporter genes in iron deficiency induced cadmium accumulation in peanut. *Front. Plant Sci.* **2022**, *13*, 894848. [[CrossRef](#)] [[PubMed](#)]
25. Tan, Z.; Li, J.; Guan, J.; Wang, C.; Zhang, Z.; Shi, G. Genome-wide identification and expression analysis reveals roles of the *NRAMP* gene family in iron/cadmium interactions in peanut. *Int. J. Mol. Sci.* **2023**, *24*, 1713. [[CrossRef](#)] [[PubMed](#)]
26. Chen, X.; Lu, Q.; Liu, H.; Zhang, J.; Hong, Y.; Lan, H.; Li, H.; Wang, J.; Liu, H.; Li, S.; et al. Sequencing of cultivated peanut, *Arachis hypogaea*, yields insights into genome evolution and oil improvement. *Mol. Plant* **2019**, *12*, 920–934. [[CrossRef](#)]
27. Panchy, N.; Lehti-Shiu, M.; Shiu, S.-H. Evolution of gene duplication in plants. *Plant Physiol.* **2016**, *171*, 2294–2316. [[CrossRef](#)] [[PubMed](#)]
28. Qian, W.; Liao, B.-Y.; Chang, A.Y.-F.; Zhang, J. Maintenance of duplicate genes and their functional redundancy by reduced expression. *Trends Genet.* **2010**, *26*, 425–430. [[CrossRef](#)]
29. Zhang, J. Genetic redundancies and their evolutionary maintenance. In *Evolutionary Systems Biology*; Soyer, O.S., Ed.; Springer: New York, NY, USA, 2012; pp. 279–300.
30. Xu, G.; Guo, C.; Shan, H.; Kong, H. Divergence of duplicate genes in exon–intron structure. *Proc. Nat. Acad. Sci. USA* **2012**, *109*, 1187–1192. [[CrossRef](#)]
31. Vasconcelos, M.; Eckert, H.; Arahana, V.; Graef, G.; Grusak, M.A.; Clemente, T. Molecular and phenotypic characterization of transgenic soybean expressing the *Arabidopsis* ferric chelate reductase gene, *FRO2*. *Planta* **2006**, *224*, 1116–1128. [[CrossRef](#)]
32. Wu, J.-X.; Liu, R.; Song, K.; Chen, L. Structures of human dual oxidase 1 complex in low-calcium and high-calcium states. *Nat. Commun.* **2021**, *12*, 155. [[CrossRef](#)] [[PubMed](#)]
33. Sun, J. Structures of mouse DUOX1–DUOX1 provide mechanistic insights into enzyme activation and regulation. *Nat. Struct. Mol. Biol.* **2020**, *27*, 1086–1093. [[CrossRef](#)]
34. Liu, R.; Song, K.; Wu, J.-X.; Geng, X.-P.; Zheng, L.; Gao, X.; Peng, H.; Chen, L. Structure of human phagocyte NADPH oxidase in the resting state. *eLife* **2022**, *11*, e83743. [[CrossRef](#)]
35. Connolly, E.L.; Campbell, N.H.; Grotz, N.; Prichard, C.L.; Guerinot, M.L. Overexpression of the *FRO2* ferric chelate reductase confers tolerance to growth on low iron and uncovers posttranscriptional control. *Plant Physiol.* **2003**, *133*, 1102–1110. [[CrossRef](#)] [[PubMed](#)]
36. Tarantino, D.; Santo, N.; Morandini, P.; Casagrande, F.; Braun, H.-P.; Heinemeyer, J.; Vigani, G.; Soave, C.; Murgia, I. AtFer4 ferritin is a determinant of iron homeostasis in *Arabidopsis thaliana* heterotrophic cells. *J. Plant Physiol.* **2010**, *167*, 1598–1605. [[CrossRef](#)] [[PubMed](#)]
37. Cao, Q.; Xu, C.; Jiang, Q.; Wang, L.; Shi, G. Comparative transcriptome analysis reveals key genes responsible for the homeostasis of iron and other divalent metals in peanut roots under iron deficiency. *Plant Soil* **2019**, *445*, 513–531. [[CrossRef](#)]
38. Duvaud, S.; Gabella, C.; Lisacek, F.; Stockinger, H.; Ioannidis, V.; Durinx, C. ExPASy, the Swiss Bioinformatics Resource Portal, as designed by its users. *Nucleic Acids Res.* **2021**, *49*, W216–W227. [[CrossRef](#)]
39. Tsirigos, K.D.; Peters, C.; Shu, N.; Käll, L.; Elofsson, A. The TOPCONS web server for consensus prediction of membrane protein topology and signal peptides. *Nucleic Acids Res.* **2015**, *43*, W401–W407. [[CrossRef](#)]
40. Mistry, J.; Chuguransky, S.; Williams, L.; Qureshi, M.; Salazar, G.A.; Sonnhammer, E.L.L.; Tosatto, S.C.E.; Paladin, L.; Raj, S.; Richardson, L.J.; et al. Pfam: The protein families database in 2021. *Nucleic Acids Res.* **2020**, *49*, D412–D419. [[CrossRef](#)] [[PubMed](#)]
41. Bailey, T.L.; Williams, N.; Misleh, C.; Li, W.W. MEME: Discovering and analyzing DNA and protein sequence motifs. *Nucleic Acids Res.* **2006**, *34* (Suppl. S2), W369–W373. [[CrossRef](#)]
42. Waterhouse, A.; Bertoni, M.; Bienert, S.; Studer, G.; Tauriello, G.; Gumienny, R.; Heer, F.T.; de Beer, T.A.P.; Rempfer, C.; Bordoli, L.; et al. SWISS-MODEL: Homology modelling of protein structures and complexes. *Nucleic Acids Res.* **2018**, *46*, W296–W303. [[CrossRef](#)]
43. Hu, B.; Jin, J.; Guo, A.-Y.; Zhang, H.; Luo, J.; Gao, G. GSDS 2.0: An upgraded gene feature visualization server. *Bioinformatics* **2015**, *31*, 1296–1297. [[CrossRef](#)]
44. Chen, C.; Chen, H.; Zhang, Y.; Thomas, H.R.; Frank, M.H.; He, Y.; Xia, R. TBtools: An integrative toolkit developed for interactive analyses of big biological data. *Mol. Plant* **2020**, *13*, 1194–1202. [[CrossRef](#)] [[PubMed](#)]

45. Lu, Z.; Zhang, Z.; Su, Y.; Liu, C.; Shi, G. Cultivar variation in morphological response of peanut roots to cadmium stress and its relation to cadmium accumulation. *Ecotoxicol. Environ. Saf.* **2013**, *91*, 147–155. [[CrossRef](#)] [[PubMed](#)]
46. Liu, C.; Yu, R.; Shi, G. Effects of drought on the accumulation and redistribution of cadmium in peanuts at different developmental stages. *Arch. Agron. Soil Sci.* **2016**, *63*, 1049–1057. [[CrossRef](#)]
47. Livak, K.J.; Schmittgen, T.D. Analysis of relative gene expression data using real-time quantitative PCR and the $2^{-\Delta\Delta CT}$ method. *Methods* **2001**, *25*, 402–408. [[CrossRef](#)] [[PubMed](#)]

Disclaimer/Publisher’s Note: The statements, opinions and data contained in all publications are solely those of the individual author(s) and contributor(s) and not of MDPI and/or the editor(s). MDPI and/or the editor(s) disclaim responsibility for any injury to people or property resulting from any ideas, methods, instructions or products referred to in the content.